White-light generation with sub-ps pulses

Anne-Laure Calendron,[1,2,*] Hüseyin Çankaya,[1,2] Giovanni Cirmi,[1,2] and Franz X. Kärtner[1,2,3]

[1] *Center for Free-Electron Laser Science, Deutsches Elektronen Synchrotron, and Department of Physics, University of Hamburg, Notkestrasse 85, 22607 Hamburg, Germany*
[2] *The Hamburg Centre for Ultrafast Imaging, Luruper Chaussee 149, 22761 Hamburg, Germany*
[3] *Department of Electrical Engineering and Computer Science and Research Laboratory of Electronics, Massachusetts Institute of Technology, Cambridge, Massachusetts 02139, USA*
**anne-laure.calendron@cfel.de*

Abstract: We generate white light supercontinuum from slightly sub-picosecond pulses at 1.03 μm and 515 nm. We compare the spectra and stability for various crystals, focusing conditions and pulse durations, and determine the best parameters for sub-picosecond driver pulse duration. Comparing the experimental observations with the theory of white-light generation from Brodeur and Chin, it appears that in this particular range of pump pulse duration, two mechanisms interact and prevent a catastrophic collapse of the beam: multi-photon excitation (typical for ~100-fs-long pulses) and avalanche ionization (typical for >1-ps pulses). The two processes both manifest themselves in different experimental observations.

©2015 Optical Society of America

OCIS codes: (320.6629) Supercontinuum generation; (320.7110) Ultrafast nonlinear optics; (190.4223) Nonlinear wave mixing.

References and links

1. A. Brodeur and S. L. Chin, "Ultrafast white-light continuum generation and self-focusing in transparent condensed media," J. Opt. Soc. Am. B **16**(4), 637–650 (1999).
2. R. R. Alfano, Q. X. Li, T. Jimbo, J. T. Manassah, and P. P. Ho, "Induced spectral broadening of a weak picosecond pulse in glass produced by an intense picosecond pulse," Opt. Lett. **11**(10), 626–628 (1986).
3. P.-A. Champert, V. Couderc, P. Leproux, S. Février, V. Tombelaine, L. Labonté, P. Roy, C. Froehly, and P. Nérin, "White-light supercontinuum generation in normally dispersive optical fiber using original multi-wavelength pumping system," Opt. Express **12**(19), 4366–4371 (2004).
4. P. L. Baldeck, P. P. Ho, and R. R. Alfano, "Effects of self, induced and cross phase modulations on the generation of picosecond and femtosecond white-light supercontinua," Rev. Phys. Appl. **22**(12), 1677–1694 (1987).
5. E. Matsubara, K. Yamane, T. Sekikawa, and M. Yamashita, "Generation of 2.6 fs optical pulses using induced-phase modulation in a gas-filled hollow fiber," J. Opt. Soc. Am. B **24**(4), 985–989 (2007).
6. J. M. Dudley and J. R. Taylor, "Ten years of nonlinear optics in photonic crystal fibre," Nat. Photonics **3**(2), 85–90 (2009).
7. G. Cerullo, A. Baltuska, O. D. Mücke, and C. Vozzi, "Few-optical-cycle light pulses with passive carrier-envelope phase stabilization," Laser Photonics Rev. **5**(3), 323–351 (2011).
8. S.-W. Huang, G. Cirmi, J. Moses, K. H. Hong, S. Bhardwaj, J. R. Birge, L. J. Chen, E. Li, B. J. Eggleton, G. Cerullo, and F. X. Kärtner, "High-energy pulse synthesis with sub-cycle waveform control for strong-field physics," Nat. Photonics **5**(8), 475–479 (2011).
9. C. Manzoni, O. D. Muecke, G. Cirmi, S. Fang, J. Moses, S.-W. Huang, K.-H. Hong, G. Cerullo, and F. X. Kärtner, "Coherent pulse synthesis: towards sub-cycle optical waveforms," Laser Photonics Rev. **9**(2), 129-171 (2015).
10. S. Fang, G. Cirmi, O. D. Mücke, S.-H. Chia, F. X. Kärtner, C. Manzoni, P. Farinello, and G. Cerullo, "*Millijoule-level parametric synthesizer generating two-octave-wide optical waveforms for strong-field experiments*," in *CLEO Pacific RIM* 2013, OSA, paper WB3–1.
11. H. Injeyan and G. D. Goodno, *High Power Laser Handbook* (MacGraw-Hill Companies 2011).
12. J. B. Ashcom, R. R. Gattass, C. B. Schaffer, and E. Mazur, "Numerical aperture dependence of damage and supercontinuum generation from femtosecond laser pulses in bulk fused silica," J. Opt. Soc. Am. B **23**(11), 2317–2322 (2006).
13. A. Brodeur and S. L. Chin, "Band-gap dependence of the ultrafast white-light continuum," Phys. Rev. Lett. **80**(20), 4406–4409 (1998).

#237207 - $15.00 USD Received 31 Mar 2015; revised 11 May 2015; accepted 12 May 2015; published 18 May 2015
© 2015 OSA

14. V. P. Kandidov, O. G. Kosareva, I. S. Golubtsov, W. Liu, A. Becker, N. Akozbek, C. M. Bowden, and S. L. Chin, "Self-transformation of a powerful femtosecond laser pulse into a white-light laser pulse in bulk optical media (or supercontinuum generation)," Appl. Phys. B: Lasers Opt. **77**(2–3), 149–165 (2003).
15. M. Bradler, P. Baum, and E. Riedle, "*Continuum generation in laser host materials towards table-top OPCPA*," in *Ultrafast Phenomena 2010*, OSA (Optical Society of America, 2010), paper ME25.
16. A. Pugzlys, P. Malevich, G. Andriukaitis, T. Floery, A. Fernandez, S. Alisauskas, A. Baltuska, L. Tan, C. F. Chua, and P. B. Phua, "*High-repetition-rate multi-millijoule femtosecond 2.1 μm Ho:YAG laser,"* in *Advanced Solid-State Lasers Congress*. 2013 (Optical Society of America, 2013), paper AF1A.4.
17. S. Coen, A. H. Chau, R. Leonhardt, J. D. Harvey, J. C. Knight, W. J. Wadsworth, and P. S. J. Russell, "White-light supercontinuum generation with 60-ps pump pulses in a photonic crystal fiber," Opt. Lett. **26**(17), 1356–1358 (2001).
18. G. Genty, S. Coen, and J. M. Dudley, "Fiber supercontinuum sources (Invited)," J. Opt. Soc. Am. B **24**(8), 1771–1785 (2007).
19. L. Berge, S. Skupin, R. Nuter, J. Kasparian, and J. P. Wolf, "Ultrashort filaments of light in weakly ionized, optically transparent media," Rep. Prog. Phys. **70**(10), 1633–1713 (2007).
20. X. W. Chen, Y. X. Leng, J. Liu, Y. Zhu, R. X. Li, and Z. Z. Xu, "Pulse self-compression in normally dispersive bulk media," Opt. Commun. **259**(1), 331–335 (2006).
21. N. Bloembergen, "The influence of electron plasma formation on superbroadening in light filaments," Opt. Commun. **8**(4), 285–288 (1973).
22. J. C. Diels and W. Rudolph, *Ultrashort Laser Pulse Phenomena (II Edition)* (Academic 2006), Chap. 3.
23. M. J. Weber, *Handbook of Optical Materials* (CRC 2003).
24. I. H. Malitson, "Refraction and dispersion of synthetic sapphire," J. Opt. Soc. Am. **52**(12), 1377–1379 (1962).
25. D. E. Zelmon, D. L. Small, and R. Page, "Refractive-index measurements of undoped yttrium aluminum garnet from 0.4 to 5.0 μm," Appl. Opt. **37**(21), 4933–4935 (1998).
26. A. Major, F. Yoshino, I. Nikolakakos, J. S. Aitchison, and P. W. E. Smith, "Dispersion of the nonlinear refractive index in sapphire," Opt. Lett. **29**(6), 602–604 (2004).
27. Y. Takeuchi, J. Kawanaka, and M. Fujita, "*Nonlinear refractive index of a YAG crystal at low temperature,"* in CLEO 2009 (Optical Society of America, 2009).
28. M. D. Levenson, "Feasibility of measuring nonlinear index of refraction by third-order frequency mixing," IEEE J. Quantum Electron. **10**(2), 110–115 (1974).
29. E. O. Smetanina, V. O. Kompanets, S. V. Chekalin, and V. P. Kandidov, "Femtosecond laser pulse filamentation under anomalous dispersion in fused silica. Part 1. Numerical investigation," Quantum Electron. **42**(10), 913–919 (2012).
30. A.-L. Calendron, H. Cankaya, and F. X. Kärtner, "High-energy kHz Yb:KYW dual-crystal regenerative amplifier," Opt. Express **22**(20), 24752–24762 (2014).
31. M. Bradler, P. Baum, and E. Riedle, "Femtosecond continuum generation in bulk laser host materials with sub-μJ pump pulses," Appl. Phys. B **97**(3), 561–574 (2009).
32. E. Yablonovitch and N. Bloembergen, "Avalanche ionization and limiting diameter of filaments induced by light-pulses in transparent media," Phys. Rev. Lett. **29**(14), 907–910 (1972).
33. R. Trebino, *Frequency-Resolved Optical Gating: The Measurement of Ultrashort Laser Pulses* (Kluwer Academic Publishers 2000).

1. Introduction

The generation of attosecond pulses is in need of few to single-cycle driver pulses, which requires octave-spanning spectra. One way of generating such broadband spectra is by supercontinuum generation in bulk [1, 2] or in fiber [3–6]. White-light generation (WLG) in bulk limits the energy of the resulting broadened pulses to a few nJ; but these low energy, broadband pulses can then be amplified by parametric amplification [7] with a high-energy pump laser. Lately high-energy, optical parametric synthesizers seeded by WLG in bulk materials have been developed to reach multi-octave spanning spectra [8–10]. Some of these synthesizers are seeded by one white light supercontinuum, which must have deterministic characteristics over the whole wavelength range of the synthesizer, such as smooth and coherent spectral coverage and phase, and high stability.

For spectroscopic applications, or for any experiment requiring data acquisition from the WLG source directly or after amplification, high repetition rates (e.g. 1 kHz) are necessary, which adds the challenge of a high average power pump. The limitations of traditional lasers like Ti:Sapphire in average power handling is overcome with the development of Ytterbium based sources [11].

Ytterbium doped materials sustain narrower emission bandwidths than Ti:Sapphire. The bandwidth amplified in the well-developed Yb:YAG laser technology corresponds to

#237207 - $15.00 USD Received 31 Mar 2015; revised 11 May 2015; accepted 12 May 2015; published 18 May 2015
© 2015 OSA

hundreds of femtosecond to picosecond pulse duration. Thus ultrafast systems based on Ytterbium pump lasers require spectral broadening, which can be realized by supercontinuum generation in bulk.

White-light supercontinuum has been demonstrated for pulse durations between sub-100 fs pulses [1, 12–14] up to 450 fs at 1 μm [15] and 550 fs at 2 μm [16], or for longer pulses with several tens of picoseconds in fibers [3, 4, 17], but not for sub-picosecond to picosecond pulses in bulk. The latter continua, generated by many picosecond long pulses, are in general incoherent [18]. Therefore, in this work, we experimentally demonstrate and study the white-light generated with pulses between 615 fs and 1.1 ps and prove its coherence, i.e. compressibility. Such pulses are readily available from Yb-based amplifiers and therefore, a small fraction of the amplified pulses can be directly used for WLG generation that is subsequently optically parametrically amplified with the remaining pulse used to pump the optical parametric amplifier (OPA). This avoids the need for synchronization between oscillator pulses generating the WLG and the amplified pulses to pump the OPA.

White-light generation in bulk with femtosecond pulses has been extensively studied [19, 20]. The spectral broadening results from the interplay of nonlinear effects during propagation through a medium: the driving laser is focused inside a crystal at intensities leading to accumulation of nonlinear effects. With self-focusing, the beam size shrinks, leading to increased intensities. The increased intensity generates plasma, freeing electrons, which defocus the beam. When the plasma defocusing compensates the self-focusing, a filament is created. During propagation, other nonlinear effects contribute to the broadening: self-steepening shortens the trailing edge of the pulse in time and leads to a broadening towards shorter wavelengths.

Self-focusing of the beam would lead to catastrophic damage if not stopped by a defocusing mechanism. For sub-hundred femtosecond pulses, this mechanism is multi-photon ionization (MPI) [21], whereas for longer pulses, self-focusing is stopped by avalanche ionization (AI) [1, 21]. In MPI, several photons with energy lower than the ionization threshold are utilized to ionize an atom; this process takes place on a sub-100 fs time scale. AI works on a longer (ps) time scale, and carriers are freed by the successive arrival of photons. Pulses with picosecond duration belong to the intermediate region and white-light continuum has not been demonstrated at this pulse duration. It is consequently of interest to understand whether a stable, reproducible and coherent spectrum can be generated from these pulses, and what mechanism underlies the supercontinuum generation (SCG). In the case of avalanche ionization stopping the self-focusing, the energy loss of the driving pulse should be noticeable and the spatial characteristics of the beam modified [1]. In the case of MPI, a strong bandgap dependence of the medium on the SCG should be observed [13].

The filament formation is influenced by several processes and parameters, such as the focusing of the driving beam and the peak power, as Ashcom *et al.* reported in [12]. The peak power is key for self-phase modulation (SPM) and self-steepening, leading to a collapse of the beam in space and time. The critical peak power for self-focusing grows quadratically with wavelength and decreases linearly with the linear and nonlinear refractive indices n_0, n_2:

$$P_{crit} = \alpha \frac{\lambda^2}{4\pi n_0 n_2}$$

where α depends on the spatial distribution of the beam and equals 1.9 for Gaussian beams [22].

From the material parameters given in Tab. 1, the critical power for YAG (sapphire) is 1.36 MW (3.26 MW) for 1 μm wavelength and 0.22 MW (0.68 MW) for 515 nm wavelength.

#237207 - $15.00 USD Received 31 Mar 2015; revised 11 May 2015; accepted 12 May 2015; published 18 May 2015
© 2015 OSA

Table 1. Comparison of the material parameters for WLG, from [23–28]: linear index of refraction n_0, nonlinear index of refraction n_2, are given for YAG and sapphire for the wavelengths λ = 1030 nm and 515 nm as well as their bandgap energy E_{gap} and zero-dispersion wavelength ZWD

	λ	n_0	n_2	E_{gap}	ZDW
	[nm]	[]	[10^{-16} cm^2/W]	[eV]	[μm]
YAG	1030	1.8153	6.5	6.3	1.6
	515	1.84	10		
Sapphire	1030	1.7552	3.06	9.9	1.315
	515	1.7731	3.3		

The ratio of peak power to critical power for self-focusing has been used in [1, 20, 29] to characterize the operating point. Typically, a ratio of P_{peak}/P_{crit} is experimentally in the order of ~1-5 for WLG in bulk [1, 14], which is similar to our experiment.

2. Experimental setup

The laser used in this experiment is a 1-kHz, 5-mJ Yb:KYW regenerative amplifier seeded with a 42.5-MHz, 1030-nm Yb:KYW oscillator [30]. A Treacy grating compressor compressed the stretched pulses to 615 fs assuming a Gaussian fit, which is close to the transform limit of 612 fs. Only a small fraction of the energy (10 μJ) was used in the experiment. The shot-to-shot energy fluctuations of the regenerative amplifier are in the order of 1.5%, measured with a photodiode. The input beam radius at $1/e^2$ is 1.0 mm and 1.7 mm in the sagittal and tangential directions.

The experimental setup, shown in Fig. 1, was composed of a telescope to demagnify the incoming beam (Tel), of the setup for white-light generation itself, including a focusing lens (L) and the crystal for WLG (X1), and of the diagnostics setup. Before the focusing lens, a variable attenuator was used to change the intensity at the crystal entrance. The numerical aperture at the entrance of the filament was varied with a set of BK7 lenses with focal lengths ranging from 50 mm to 200 mm. An iris located before the focusing lens allowed to finely adjust the input beam diameter, i.e. the focused beam diameter and the numerical aperture, as described in [12]. This variation was kept to the minimum to avoid diffraction effects in the focus.

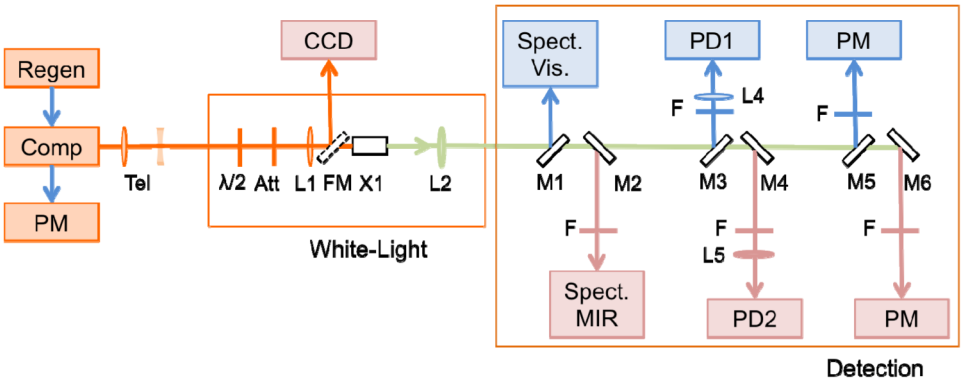

Fig. 1. Layout of the setup for characterization of white-light generated with sub-picosecond pulses. PM: powermeter, FM: flip-mirror, PD: photodiode, Spect: Spectrometer, X1: crystal, M1 to M6: mirrors, L1 to L4: lenses, Att: attenuator, F: filter sets.

For the measurements of the WL generated with 515 nm driving wavelength, a supplementary second harmonic generation (SHG) stage was added after the compressor. The SH was generated with a 1.5 mm long BBO crystal and separated from the fundamental frequency with three dichroic mirrors. The energy after the SHG stage was 1 mJ, from which only a few μJ were used for this experiment.

#237207 - $15.00 USD Received 31 Mar 2015; revised 11 May 2015; accepted 12 May 2015; published 18 May 2015
© 2015 OSA

Table 2 gives the experimental parameters of the driving laser for each lens: spot sizes in x and y, and divergences; depending on the exact input energy, the corresponding intensities were between 26 GW/cm^2 and 270 GW/cm^2, fluences between 16 mJ/cm^2 and 166 mJ/cm^2 whereas the ratios peak power over critical power were between 0.96 and 1.47.

Table 2. Experimental parameters of the driving laser: focal lengths, calculated spot sizes in x and y directions and divergences.

Focal length	Spot size		Divergence
	x	*y*	
mm	*µm*	*µm*	*mrad*
200	64	39	7
100	32	19	14
75	24	14	18
60	19	12	22
50	16	10	26

The diagnostic setup covered the broadest possible wavelength region, from the visible to the infrared. For this reason, two spectrometers and two photodiodes have been used: the detection in the visible was performed with an HR4000 spectrometer from OceanOptics covering the range from 200 nm to 1100 nm and with a GaAs photodiode EOT4000; in the IR, the spectrometer used was a NIRQuest 256 from OceanOptics ranging from 900 nm to 2500 nm and an InGaAs detector Det10D/M from Thorlabs. Except for the visible spectrometer measuring the visible continuum driven by 1030 nm pulses, a set of filters was placed to suppress the fundamental spectrum, however reducing the signal level and preventing to record the whole spectral coverage; this is the origin of the hole between pump and IR broadening shown in Fig. 2(a). This has the advantage of resolving the visible supercontinuum without introducing the losses and potential ripples of short pass filters. During the measurement of the 515 nm driven WLG however, the spectra of the visible and IR continua were acquired after 500 nm short pass and 550 nm long pass filters, respectively.

The materials used in this WLG study are 6 and 10 mm thick YAG, 6 mm thick sapphire and 6.35 mm thick CaF_2 crystals. As sapphire is birefringent, the broadening depends on the orientation of the polarization with respect to the crystallographic axes. A half-waveplate was added in the input beam path to rotate the polarization. The intensities are calculated in the foci, taking into account the Fresnel losses for normal incidence on the crystals.

The optimization criterion was the generation of the broadest spectra with less than 5% fluctuations in the two spectral regions below and above the pump wavelength, referred to as visible and IR broadening and shown in Fig. 2(a). The filters used to suppress the pump wavelength range determine the lower and upper wavelength regions. The broadened spectral wing exhibits a smooth spectrum and the spectral broadening close to the driver wavelength is due to SPM. The visible spectrum shows thus a dip with low spectral density and it is convenient to define the lower spectral region up to this wavelength. In the following measurements this dip was located at 900 nm, as indicated in Fig. 2(a).

Experimentally, two domains along the propagation axis were found with a single filamentation: in the first one, corresponding to a shorter distance between lens and crystal, the broadening extends mainly toward the visible, whereas the second one is correlated with a significantly broader and more stable continuum toward the IR. The minimization of amplitude fluctuations for both spectral regions simultaneously was possible only in the second filament position, however the complexity of the alignment and its robustness against external influences greatly depend on the exact experimental parameters (lens, pump energy).

The exact behavior of the filament between both domains strongly depends on the exact focusing conditions and input energy: either the transition between both domains is smooth, or there is a transition with multi-filamentation. The behavior of the divergence of the filament can be explained by the guiding of the filament over different lengths: the first

#237207 - $15.00 USD Received 31 Mar 2015; revised 11 May 2015; accepted 12 May 2015; published 18 May 2015
© 2015 OSA

domain corresponds to a focus position further inside the crystal than in the case of the second domain [1]. This is in agreement with the observation that the continuum was starting very close to the surface of the crystal in the case of a 6 mm crystal; the focusing of the input beam onto the surface during the optimization of the alignment lead repeatedly to damage of the crystal in this configuration.

In the analysis, the response functions of the filters, lens coatings, silver mirrors, powermeters and spectrometers have been taken into account for rescaling energies and spectra.

A measurement with one configuration (10 mm YAG-crystal and 100 mm focal length lens) has been repeated 10 times for the calculation of error bars. During each measurement, the lens has been removed and the incoming beam misaligned; realigning the WL shows then the influence and reproducibility of the position of the lens and the angle of incidence on the crystal. The error was taken as the standard deviation σ.

3. Influence of the material

In this section, we first compare the results obtained with the 6-mm long sapphire and YAG crystals, then we focus on the differences in the WL for 6 and 10 mm long YAG crystals. These crystals produced the best WL under different focusing conditions. At the end, the results obtained with a 515 nm drive laser will be presented and discussed.

For each crystal, the setup has been optimized in the following way: the focusing lens has been exchanged, its position varied and the variable attenuator adjusted to find the optimum numerical aperture, start position of the filament and intensity, respectively.

3.1 Comparison of WLG from sapphire and YAG

At 1030 nm, stable WL super-continua have been generated with all three materials. The CaF_2 crystal degraded however very quickly and for this reason the results with CaF_2 at 1030 nm are not presented here. The set up with a 100 mm focusing lens, a 10 mm long YAG crystal and a 2.7 mm input beam diameter presented the least sensitivity to experimental variations such as crystal position and intensity.

Figure 2 shows the measured WL continua for the 6-mm long YAG and sapphire crystals, rescaled so that the area corresponds to the measured energy for the visible and IR continua.

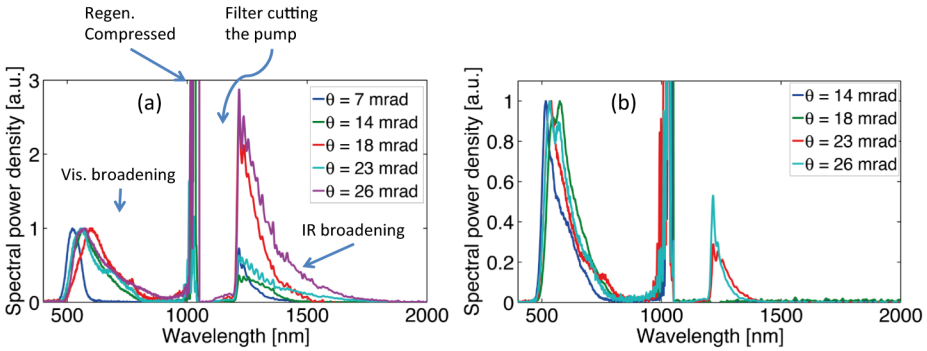

Fig. 2. WL-supercontinua obtained with 6 mm YAG (a) and sapphire (b) under different focusing conditions. On (a), the broadening toward the visible and the infrared as well as the driving pulses and the spectral hole due to the filtering of the driver are indicated.

Figure 3 shows the evolution of the spectral width at 5% of the maximum amplitude versus divergence, and Fig. 4 displays the evolution of power vs. intensity and divergence of the input beam. In all graphs the characteristics of both visible and IR -continua are shown as blue and red lines, respectively.

#237207 - $15.00 USD Received 31 Mar 2015; revised 11 May 2015; accepted 12 May 2015; published 18 May 2015
© 2015 OSA

The intensity in the crystal at focus was determined using the measured diameter of the collimated input beam in x- and y-direction, propagation with ABCD formulas through the focusing lens and using the measured distance between the middle of the thin lens and the crystal surface. The precision in distance measurements has been included in the calculation of the error bars of the intensity.

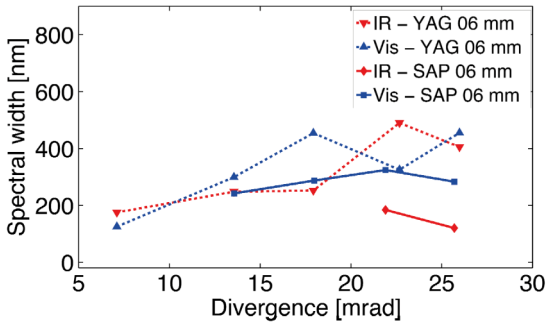

Fig. 3. Spectral width of visible (blue) and IR (red) continua obtained with 6 mm YAG (dashed) and 6 mm sapphire (solid). The full spectral width is taken at 5% from the maximum amplitude of each wing.

An increase in spectral width of the SCGs with increasing divergence is observed, which may be related to an increase of energy coupling into the filament. Moreover, a stronger focusing induces a smaller focused spot size, i.e. the broadening due to accumulation of nonlinear phase increases. In analogy with continuum generation in a waveguide, the higher the energy coupled into it, the larger is the broadening. This is also confirmed in Fig. 4 by the increase of power with divergence.

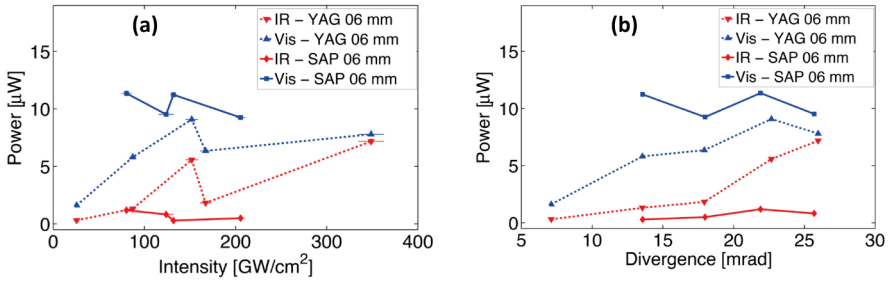

Fig. 4. Power contained in the visible and IR- continua, vs. intensity (a) and divergence (b) of the input beam. The crystals used here were YAG and sapphire, each 6 mm long.

A trend in the broadening of the driving pulses is observed: the power is always higher in the visible than in the IR continuum. This is even more pronounced with sapphire than with the YAG crystal. In sapphire, the IR continua are rather weak, and sometimes even not measurable with our experimental setup when using the 75 mm and 100 mm lenses, corresponding to spot sizes at focus in the crystal larger than 15 µm. The total power measured in the filaments created in YAG or sapphire is similar in the visible region, but differs in the IR region easily by one order of magnitude. This different behavior, which was also reported in [31], might originate from a too short filament in the 6 mm long sapphire crystal compared with the 6 mm long YAG crystals, considering the long pulse duration and narrow-band input spectrum of the driver laser. In the case of sapphire no broadening was observed for the largest spot sizes: in this case, the focusing was probably too loose to start accumulating nonlinearities via self-phase modulation and to shorten the pulse in time via self-steepening. As indicated in Tab. 1, the nonlinear index of sapphire is about half that of

#237207 - $15.00 USD Received 31 Mar 2015; revised 11 May 2015; accepted 12 May 2015; published 18 May 2015
© 2015 OSA

YAG, i.e. the accumulation of nonlinear phase in sapphire is half that in YAG under the same propagation conditions.

The low conversion efficiency from the driving laser into the supercontinuum, less than 5%, is a sign that the mechanism of ionization is probably not AI but MPI [1, 32]. Moreover, no measurable loss in total transmitted pulse energy was found, which is also a sign of MPI [1].

The short wavelength cut-off is located between 460 nm and 490 nm in YAG, decreasing with intensity and is reproducibly equal to 475 nm in all configurations obtained with the sapphire crystal, as we can see from Fig. 2. As can be seen from the continua generated from Sapphire and YAG, the precise cut-off depends on the material and therefore on material band-gap and on excitation conditions, as has been also observed in [13].

3.2 Influence of the material length: in case of YAG

Figure 5 shows the continua obtained for the 10 mm long YAG crystal. In a similar way as in the previous section, Fig. 6 and 7 show the evolution of spectral bandwidth and power of the visible and IR-continua vs. intensity and peak power, comparing the 6 mm and 10 mm long YAG crystals. The visible continuum is here also normalized to 1, in order to show the change in amplitude of the IR continuum for the different focusing conditions. The broadest spectra with the lowest fluctuations (<1% rms) have been obtained with the longer crystal of 10 mm with 14 mrad and 18 mrad divergence of the input beam.

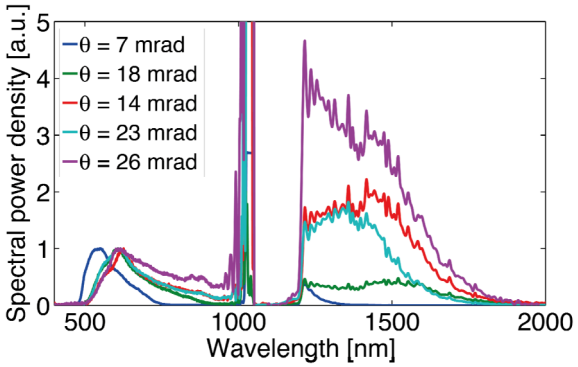

Fig. 5. WL-supercontinua obtained with 10 mm YAG crystal for different focusing conditions of the driver pulses.

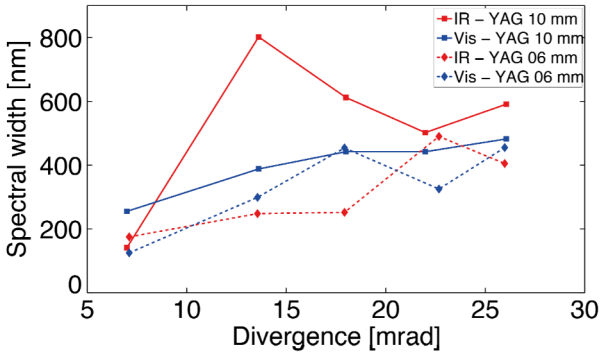

Fig. 6. Spectral width calculated at 5% of the maximum amplitude of the visible and IR-continua obtained with 10 mm and 6 mm YAG crystals.

#237207 - $15.00 USD Received 31 Mar 2015; revised 11 May 2015; accepted 12 May 2015; published 18 May 2015
© 2015 OSA

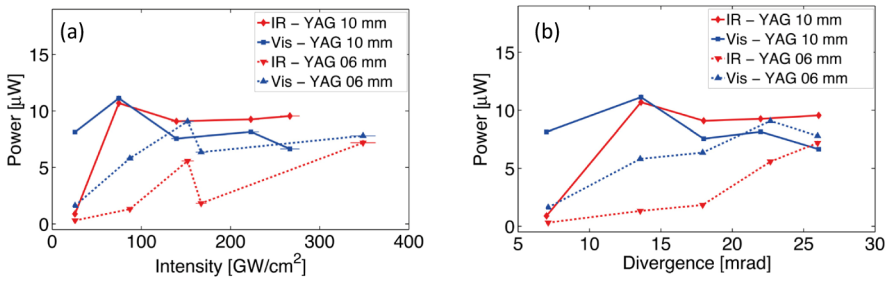

Fig. 7. Power contained in the visible and IR supercontinua, vs. intensity (a) and divergence (b) of the input beam, for 6 mm and 10 mm YAG crystal lengths.

With the short YAG crystal the generated IR power is lower than with the longer YAG crystal, as can be seen in Fig. 7(a). In Fig. 7(b), the width of the continua and their corresponding power content converge to a similar value under strong focusing for both crystal lengths. This corresponds to a saturated filament in the 10 mm long crystal and a transient filament in the 6 mm long crystal, which reaches saturation only under strong focusing condition. The broadening generated in the 6 and 10-mm long YAG crystals also differ, as can be seen in Fig. 5 and 6, the spectral width achievable from the longer crystal varies strongly over the different experimental configurations, but it is constant in the case of the shorter crystal, being equal to the width obtained under loose focusing conditions with the longer crystal.

Using a longer lens, f = 200 mm, corresponding to an increased spot size of 50 µm and the lowest NA, the spectra from both 6 mm and 10 mm long YAG crystals are drastically narrower than with tighter focusing. Interestingly, in this focusing configuration, the cutoff reaches 480 nm with the longer crystal whereas it reaches only 505 nm with the stronger focusing conditions, at the onset of a saturated filament, as can be seen from Fig. 5. The cutoff reaches only 500 nm for the configurations with the 10 mm-long YAG crystal and spot sizes below 25 µm; for the larger spot size of 50 µm, the cutoff is located at 480 nm.

In conclusion, the supercontinua in the visible and in the IR were smoother, broader and more stable with YAG than with sapphire. Even if the spectra look similar for the two crystal lengths, the longer YAG crystal generated more robust continua against disturbances such as thermal changes of the environment or air flow than the shorter crystal.

3.3 Observations on the spatial profile of the driving beam

The pump profile has been measured with a CCD camera after the crystal, with and without the filament, as shown in Fig. 8. There is a clear change in beam profile. The filament has been filtered to isolate the pump. When the filament appears, the beam profile of the driving beam is modified and a weak side-lobe appears, at the same position than the filament. A change in beam profile of the driving laser is typically correlated with avalanche ionization [1].

As AI starts typically from a defect in the crystal, we translated the crystal transversally to the propagation direction and verified that this change is actually independent of the beam position on the crystal. A possible explanation of the change in the beam profile might then be the influence on the filament formation of the spatial characteristics of the beam, which is slightly astigmatic.

#237207 - $15.00 USD Received 31 Mar 2015; revised 11 May 2015; accepted 12 May 2015; published 18 May 2015
© 2015 OSA

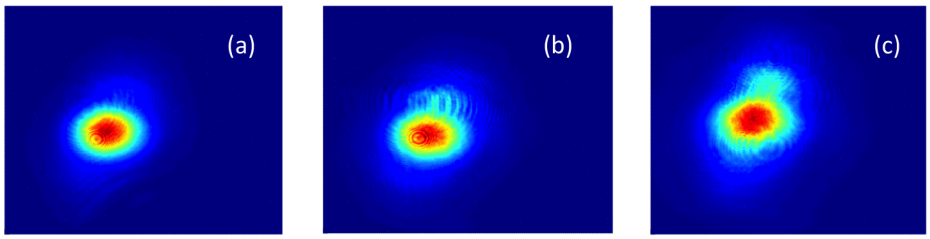

Fig. 8. Driving beam profile measured after the crystal in 3 configurations: without filament (a), at the threshold of filamentation (b) and for the established filament (c). Profiles were taken by reducing progressively the IR input power from the settings for a stable filament down to vanishing of the filament.

3.4 Results for 515 nm driving pulses

For a pump wavelength of 515 nm, broadening has also been observed. The broadening was limited towards the UV by the absorption edge of the material. The spectra obtained with compressed pulses are shown in Fig. 9.

Strongly different behavior is observed with both the YAG and sapphire crystals. Spectral broadening could be obtained with both crystals, but only for a limited range of focusing conditions, indicated in Fig. 9. With CaF_2, the broadening was significant, but the crystal degraded immediately. This different behavior is due to the material bandgap, as explained in [13]; for CaF_2, the absorption edge is lower than for sapphire and YAG. In the WLG process, the absorption of the extreme spectral components prevents further four-wave mixing and thus limits the broadening. A strong absorption in the UV leads to damage of the material.

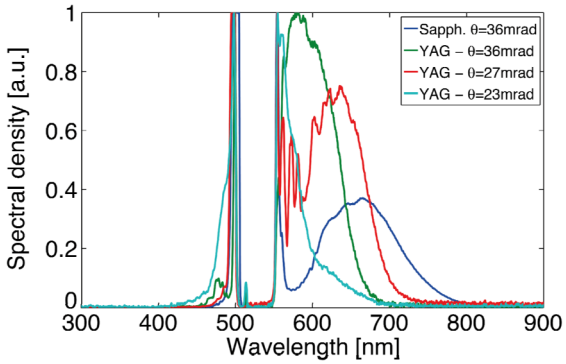

Fig. 9. Supercontinua obtained with 515 nm driving pulses in 6 mm long sapphire and YAG crystals. In the case of YAG, 3 different focusing conditions lead to different spectral broadening.

During the spectral measurements of white-light driven with 515 nm or 1030 nm pulses, we looked for a bandgap dependency, which would be a sign of MPI stopping the collapse, but no clear dependency was noticeable, only a trend which was stronger in the case of 515 nm driving pulses.

4. Influence of pulse duration

After studying the influence of the material onto WLG, the influence of the pulse duration has been investigated in two ways, first by changing the compression of the driving pulses, second by narrowing their spectrum.

Changing the distance between gratings in the compressor introduces positive or negative chirp on the pulses. The spectral bandwidth was cut in the compressor to increase the pulse duration while maintaining a transform-limited pulse.

#237207 - $15.00 USD Received 31 Mar 2015; revised 11 May 2015; accepted 12 May 2015; published 18 May 2015
© 2015 OSA

For these measurements, the 10 mm long YAG crystal with a 75 mm focal length lens was chosen. The pulse duration was monitored by an intensity autocorrelator. Assuming a Gaussian pulse [30], the pulse widths derived varied between 615 fs, 1030 fs and 1070 fs corresponding to the compressed, positively and negatively chirped pulses, respectively.

Figure 10 shows the obtained spectra, spectral width and power of the visible and IR continua as a function of chirp. The shape of the spectra, thus the spectral widths, remained similar for all measurements, as can be seen in Fig. 10(a) and 10(b). The power however tends to depend on the pulse duration, as indicated in Fig. 10(c): the power in the visible domain increased slightly for longer pulses, positively and negatively chirped, whereas the one in the IR tend to decrease. Figure 10(c) shows, that minimum fluctuations have been obtained with the shortest, transform-limited pulse duration. We obtained a very good stability with energy fluctuations <1% rms. The spectral width remained constant for negatively chirped pulses, but tends to decrease in the visible for positively chirped pulses.

Albeit similar spectral shapes and measurable energy fluctuations, the SC obtained with shorter pulse durations was more robust against environmental disturbances than the one obtained with stretched pulses. This might be compensated with a longer crystal to saturate the filament generated with longer pulses, in a similar way than the demonstration in the previous section showing the scaling from more traditional, few 100s fs long pulses to sub-picosecond pulses. These differences might be at first surprising, considering the relatively low amount of dispersion, but this corresponds to a doubling of the pulse duration.

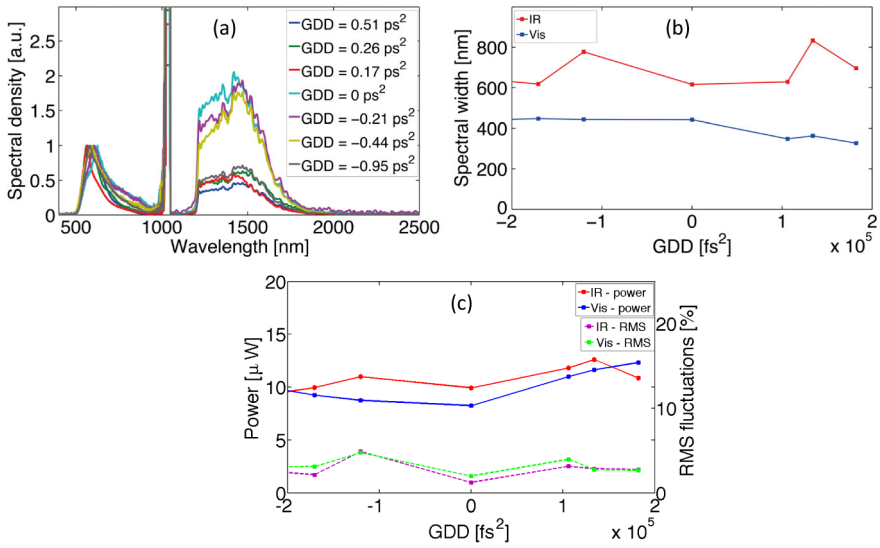

Fig. 10. Influence of chirp on the WLG. The WL-continua are shown in (a), the evolution of spectral width for visible and IR-continua are shown in (b) and the power and rms stability as a function of group delay dispersion in (c). The solid lines show the power evolution whereas the dashed curve displays the rms stability.

When increasing the pulse duration while keeping the pulses transform-limited, a similar trend was observed: the spectral shapes remained relatively constant, as shown in Fig. 11(a) and 11(b), while the power of both visible and IR continua increases slightly, as can be seen in Fig. 11(c). The filament was however difficult to stabilize for narrowband, long pulses, and we suppose that a longer crystal would have been necessary to reach saturation. This is correlated with the increase of the rms fluctuations with the narrowing of the spectral width.

#237207 - $15.00 USD Received 31 Mar 2015; revised 11 May 2015; accepted 12 May 2015; published 18 May 2015
© 2015 OSA

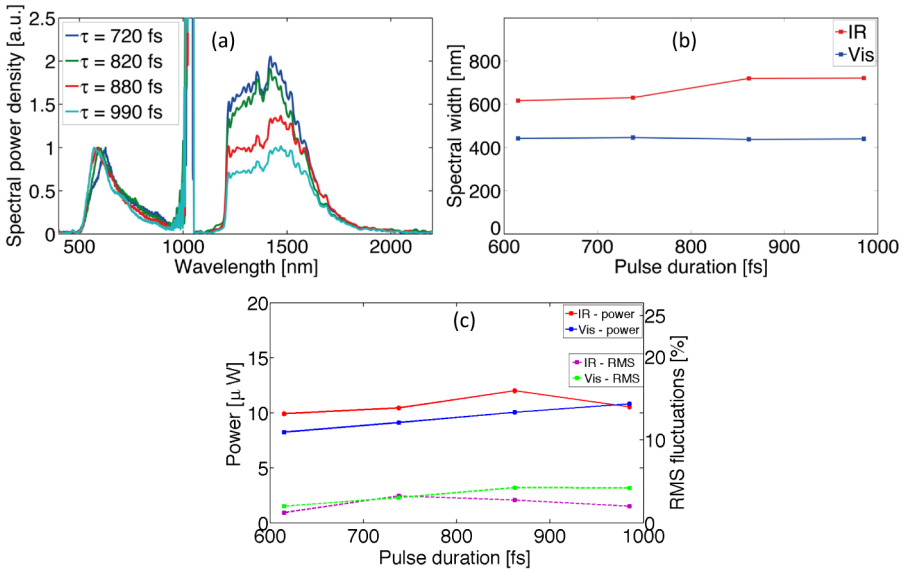

Fig. 11. Influence of the transform-limited pulse duration on the WLG process. The generated continua are shown in (a), the evolution of the spectral width in (b), and the power and rms stability vs. dispersion in (c). The solid lines show the power evolution whereas the dashed curve displays the rms stability.

In both cases of longer pulses, either stretched or transform limited, the filament was beginning almost at the surface of the crystal, leading to intensities on the surface close to damage threshold.

In summary, the best parameters to generate a stable, broadband white-light supercontinuum in a 10-mm-long YAG crystal from 1030-nm pulses corresponds to an intensity of ~8 GW/cm^2, a numerical aperture of 0.015 using 100 mm focal length lens for an input beam diameter of 2.7 mm and transform limited pump pulses. In our experiment, the shortest pulse duration has lead to the most stable and broadest continua.

5. Spectral phase-measurement

Now, we turn to the question of coherence of the generated WL-supercontinuum, which could limit its compressibility. This is especially problematic when long driving pulses and consequently longer crystals are used. To verify compressibility we measure its spectral phase. The low energy of the generated WL, on the order of 10 nJ, makes this measurement difficult at 1 kHz repetition rate, without prior amplification of the spectrum. For this reason, part of the WL-continuum has been parametrically amplified to the μJ level. The amplified bandwidth is limited by the crystal length and the phase-matching bandwidth of the nonlinear crystal (BBO). We then used second-harmonic frequency resolved optical gating (SH-FROG) [33] to measure the spectral phase of the amplified pulses.

By angular tuning of the parametric amplifiers, the amplified spectral region can be tuned between 1550 nm and 2400 nm. We performed FROG measurements on different spectral regions to verify the compressibility of the phase.

Figure 12 shows the results obtained for the spectral coverage between 1700 nm and 1800 nm, corresponding to 35 nm FWHM wide signal pulses centered at 1.76 μm. The retrieved 33.2 nm wide pulses are 197 fs long. The measured spectrum and the reconstructed one perfectly agree with each other after marginal correction compensating for the calibration of the spectrometers. The spectral phase is well-behaved and compressible. The Fourier-transform of the measured spectrum is 53 fs long. The compression to the Fourier-limit has

#237207 - $15.00 USD Received 31 Mar 2015; revised 11 May 2015; accepted 12 May 2015; published 18 May 2015
© 2015 OSA

not been implemented in this work, as the uncompressed pulses are used for further experiments.

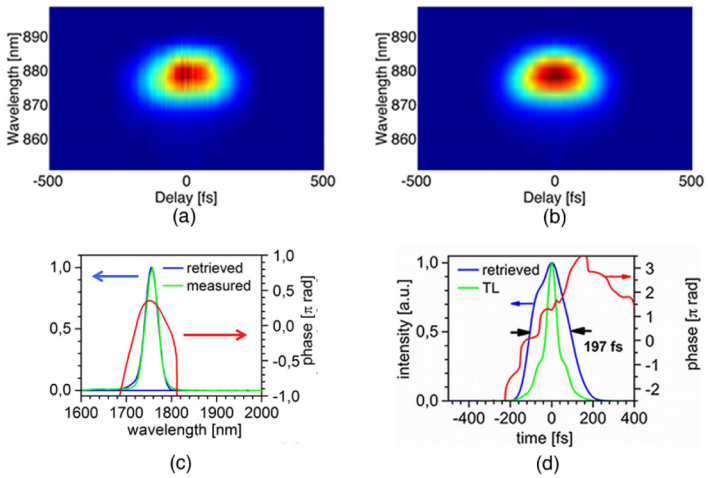

Fig. 12. FROG measurement of the signal pulses after the second OPA. The measured (a) and retrieved (b) FROG traces are shown in the first row and the retrieved spectral (c) and intensity (d) profiles in the second row (TL, transform limited).

6. Conclusions

We investigated WLG with slightly sub-picosecond driving pulses and optimized focusing conditions and pulse parameters such as numerical aperture and intensity for different materials. WLG from sub-picosecond pulses is particularly interesting from the physical point of view, since this duration lies in the intermediate regime between ~100 fs pump pulses, in which the dominant defocusing mechanism stopping self-focusing is MPI, and >1 ps pulses, in which the dominant process is instead AI. Some of the observations, the negligible decrease in pump energy (i.e. low conversion efficiency of the pump into the supercontinuum), presented in this paper seem to imply a dominant MPI mechanism. On the other side, the observation that the beam profile is slightly modified at the onset of WLG is more consistent with defocusing due to A.I. Varying the focusing parameters did not show a clear influence on the short wavelength cutoff: in the case of a dominant MPI mechanism, a dependency on the material bandgap only would have been expected, and on the pump parameters in the case of the dominant AI mechanism [1,13].

The three observations, apparently in contradiction with one another, are consistent with the intermediate duration of our pump. There does not seem to be a dominant defocusing process in this case, but the two processes (MPI and AI) are both simultaneously influential. A deeper understanding can be pursued by detailed simulations, which is not attempted here.

As a result, we obtain very stable (<1% energy fluctuations) white light supercontinua covering 500 nm to 2.5 μm, pumped by 615-fs-long Yb-laser pulses. After comparing three materials and optimizing conditions, this broadest, most stable and robust supercontinuum was obtained with a 10 mm long YAG-crystal, an intensity of 8 GW/cm^2, 0.015 mrad divergence and the shortest possible pulse duration (615 fs). FROG characterization of a spectral part of the white light, amplified with two OPAs, shows that the phase is well-behaved and compressible.

This result shows that the well-known WLG in bulk with ~100 fs long pulses is scalable to sub-picosecond driving pulses by adapting focusing conditions and material length; one major difference lies in the need to compress the pulses at the input of the crystal to ensure sufficient accumulation of nonlinear effects to start the filamentation process. The

#237207 - $15.00 USD Received 31 Mar 2015; revised 11 May 2015; accepted 12 May 2015; published 18 May 2015
© 2015 OSA

demonstrated sub-ps-pumped supercontinnuum is a suitable seed for a high-energy parametric waveform synthesizer.

Acknowledgments

This work was supported by the excellence cluster "The Hamburg Centre for Ultrafast Imaging–Structure, Dynamics and Control of Matter at the Atomic Scale" of the Deutsche Forschungsgemeinschaft, the ERC-Synergy grant AXSIS with grant no. 609920. The authors acknowledge helpful discussions with Dr. Joachim Meier, Ara Choudhuri, Dr. Axel Rühl, and Giulio M. Rossi.

#237207 - $15.00 USD Received 31 Mar 2015; revised 11 May 2015; accepted 12 May 2015; published 18 May 2015
© 2015 OSA